Supplementary Information

A versatile interpenetrating polymer network approach to robust stretchable electronics

Guoyan Zhang[1,2], Michael McBride[1], Nils Persson[1], Savannah Lee[1], Tim J. Dunn[3], Michael F. Toney[3], Zhibo Yuan[4], Yo-Han Kwon[1], Ping-Hsun Chu[1,§], Bailey Risteen[1], Elsa Reichmanis[1,4,5]*

[1]School of Chemical and Biomolecular Engineering, Georgia Institute of Technology, Atlanta, GA 30332, USA. [2]College of Engineering, Peking University, Beijing, 100871, P. R. China. [3]Stanford Synchrotron Radiation Light source Menlo Park, CA 94025, USA. [4]School of Chemistry and Biochemistry, Georgia Institute of Technology, Atlanta, GA 30332, USA. [§]Current address: Intel Corporation, 2501 NE Century Blvd, Hillsboro, OR, 97124, USA. [5]School of Materials Science and Engineering, Georgia Institute of Technology, Atlanta, GA 30332, USA. e-mail: elsa.reichmanis@chbe.gatech.edu.

Text:

Materials

The processing solvent chloroform ($CHCl_3$, anhydrous, ≥ 99%, containing 0.5-1.0% ethanol as stabilizer) was purchased from Sigma-Aldrich and used as received. For the commercial semiconductors, Poly(3-hexylthiophene-2,5-diyl) (P3HT, Mw: 90 kDa, Regioregularity: 96%) was purchased from Rieke Metals Inc.; Poly[2,5-(2-octyldodecyl)-3,6-diketopyrrolopyrrole-alt-5,5-(2,5-di(thien-2-yl)thieno [3,2-b]thiophene)] (DPP-DTT, Mw: 292,200, Mn: 74, 900, PDI: 3.90) and Poly(2,5-bis(2-octyldodecyl)-3,6-di(pyridin-2-yl)-pyrrolo[3,4-c]pyrrole-1,4(2H,5H)-dione-alt-2,2'-bithiophene) (DPPDPyBT, Mw: 20,310, Mn: 12, 030, PDI: 1.69) were purchased from Ossila Ltd and used without further purification. Poly(dimethylsiloxane) (PDMS, Sylgard 184) and Silicone removing solvent (DS-2025) were purchased from Dow Corning. Ecoflex gel (0035) was purchased from Nelson A. Burke Co., LLC. PEDOT: PSS (PH1000) was obtained from Clevious. Poly(styrenesulfonate)-bis(trifluoromethane) sulfonimide lithium salt (LiTFSI, 99.95% trace metals basis) was purchased from Sigma-Aldrich.

Methods and characterization

Stretchable, Transparent interpenetrating semiconducting polymer network film fabrication and characterization

The commercial semiconductor solutions (5 mg/mL) for the semiconducting film were prepared by dissolving the commercial conjugated polymers and PDMS (w_{base}:$w_{cross\text{-}linker}$ = 10:1) with designated weight ratios in $CHCl_3$ at 55 ^oC for 30 min and then cooled down to room temperature (RT). The solutions were directly spin-coated onto 300 nm SiO_2 substrates at 1500 rpm for 60 s, and then annealed at 160 ^oC for 1 h. For the freestanding films, the solutions were poured into a mold and cured at 55 ^oC for 4 h. For the characterization, films on different substrates were prepared. Films on glass slides were used for UV/vis/NIR spectroscopy, optical microscopy, atomic force microscopy (AFM) and X-ray photoelectron spectroscopy (XPS); silicon substrates were used for Grazing-Incidence Wide-Angle X-ray Scattering (GIWAXS) and scanning electron microscopy (SEM) analysis. Additionally, PDMS substrates were utilized for the evaluation of mechanical properties and electronical properties under large strain. The solution and film UV-vis spectra were recorded using an Agilent 8510 UV-vis spectrometer. The surface morphologies of the films were characterized by AFM using a Bruker Dimension Icon atomic force microscopy system, operating in tapping mode with a silicon tip (TAP150, Bruker). Scanning electron microscope (SEM) measurements were performed with a Zeiss Ultra60 FE-SEM scanning electron microscope whereby the measurement parameters were set as 10 kV for the accelerating voltage and 10 μA for the current. The GIWAXS measurements were carried out on beamline 11-3 at the Stanford radiation light source. The beam was fixed at an energy of 12.7 keV and the critical angle was 0.12°. X-ray photoelectron spectra were obtained using a K-Alpha XPS system with a focused monochromatic Al KR X-ray

source for excitation and a spherical section analyzer. Mechanical tensile-stress experiments were performed using an Instron 5567 instrument at room temperature (25 °C). The delamination-stretching-relamination process whereby semiconducting films were fabricated on OFET substrates, and then delaminated, stretched and finally while stretched, relaminated back onto an OFET substrate, was used to evaluate the electrical performance durability of the elastic semiconducting films under strain using an Agilent 4155C semiconductor parameter analyzer.

Fully stretchable transistor arrays fabrication and characterizations

The device fabrication started with a Si/SiO_2 wafer with the desired pattern (**Video S3-1**). PDMS solution (20 mg/mL in $CHCl_3$) was spin coating on the wafer as adhesion layer (**Video S3-2**). PEDOT: PSS-LiTFSI solution was prepared as reported previously and spin-coated on the wafer 1 (**Video S3-3**), followed by removing the photoresist layer using acetone and leaving only the PEDOT: PSS-LiTFSI on the PDMS adhesion layer (**Video S3-4**). Semiconductor/PDMS mixture was subsequently spin-coated onto these layers to form a self-encapsulating active material-dielectric layer (**Video S3-5**). Gate electrodes were prepared by spin-coating PEDOT: PSS-LiTFSI solution onto the above layers (**Video S3-6**). Then a mixture with 15 wt% of PDMS in Ecoflex gel (w_{partA}:w_{partB} = 1:1) was poured onto the top the device (**Video S3-7**), followed by 4 h curing at 55 °C (**Video S3-8**). Finally, the source-drain electrode layer, active-dielectric layer together with the gate electrode layer were peeled off with the PDMS/Ecoflex substrate from the Si wafer (**Video S3-9 and 10**).

Figures and Tables.

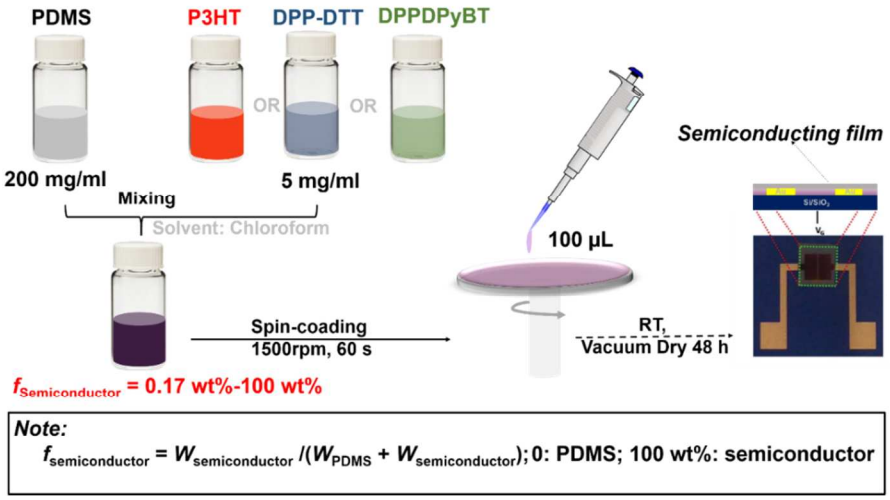

Fig. S1. Schematic illustration of the fabrication steps for the semiconducting film on silicon wafer with gold as electrode.

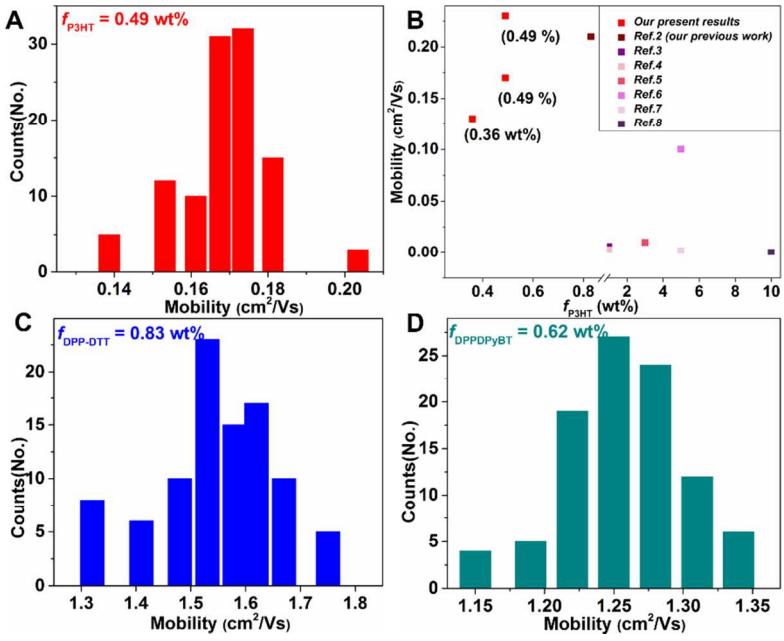

Fig. S2. Summary of devices characteristics for 100 transistors in different batches: **A**: P3HT (0.49%), **C**: DPP-DTT (0.83%), **D**: DPPDPyBT (0.62%). Comparison of the obtained mobilities (red square) at low weight fraction of P3HT in this study to previously reported results in the literature (**B**) 2-8.

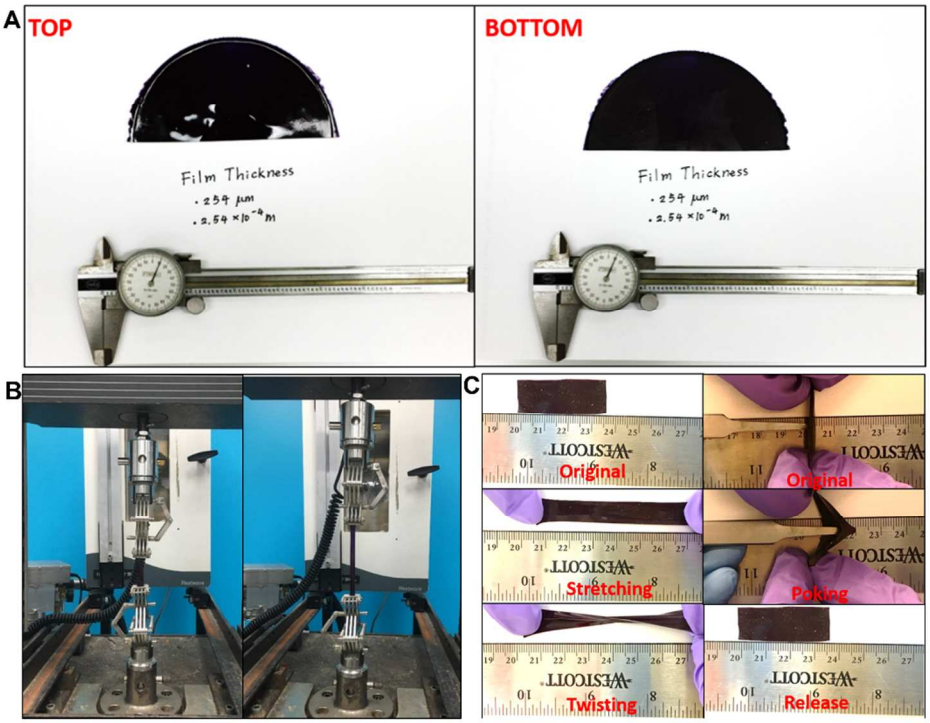

Fig. S3. Top and bottom photographs of a semiconducting film with 0.49% P3HT (**A**). Photographs of the semiconducting film (0.49 wt% of P3HT) before and after stretching (**B**). Photographs of the freestanding films (0.49 wt% of P3HT) being stretched, twisted and poked (**C**).

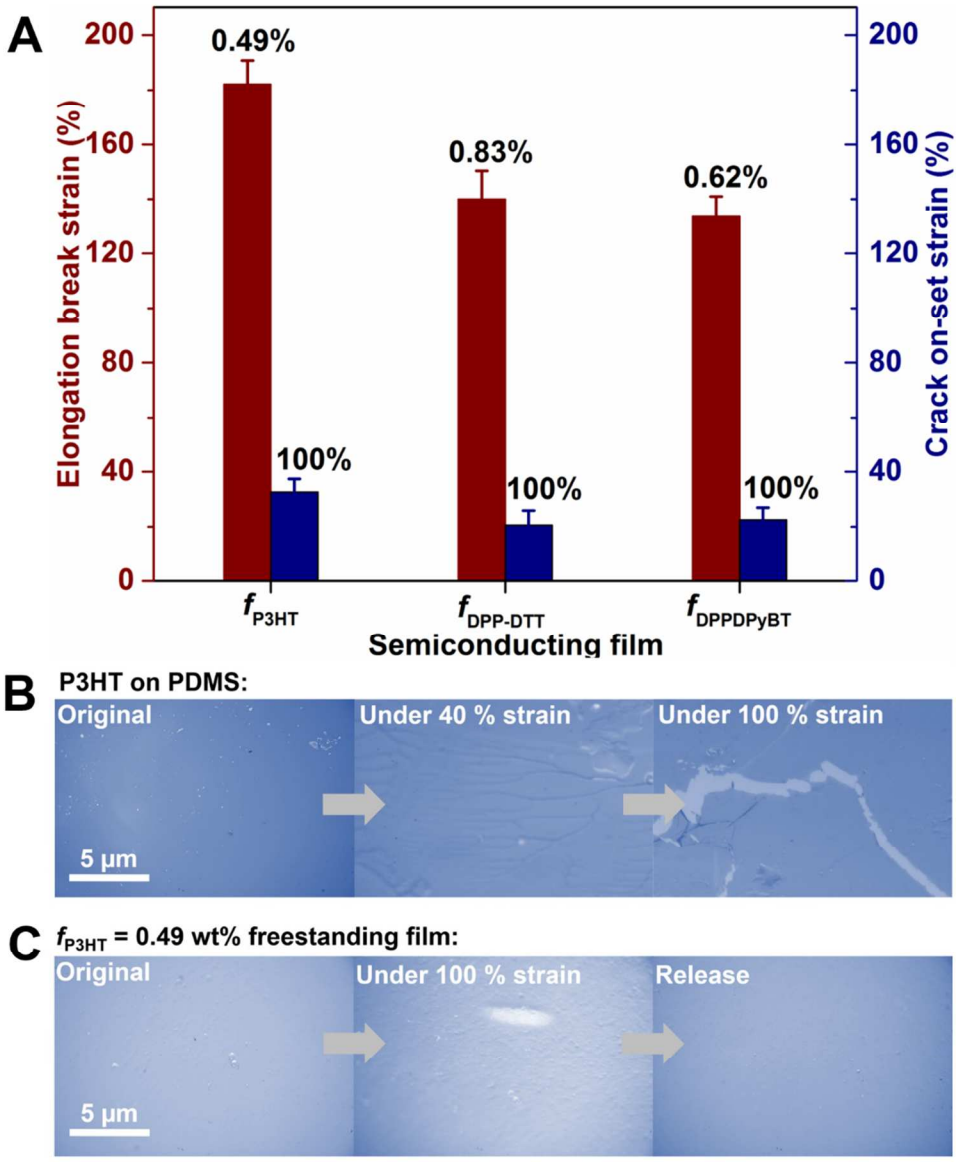

Fig. S4. Elongation break strain of the freestanding semiconducting films under optimized weight fraction and crack on-set strain of the neat semiconductor film on PDMS substrate 9, 10. The error bars represent the range of measurement error (**A**). Optical micrographs of the neat P3HT film on PDMS substrate under original, 40% strain and 100% strain conditions (**B**). Optical micrographs of the freestanding semiconducting film with 0.49% P3HT under original, 100% strain and release conditions (**C**).

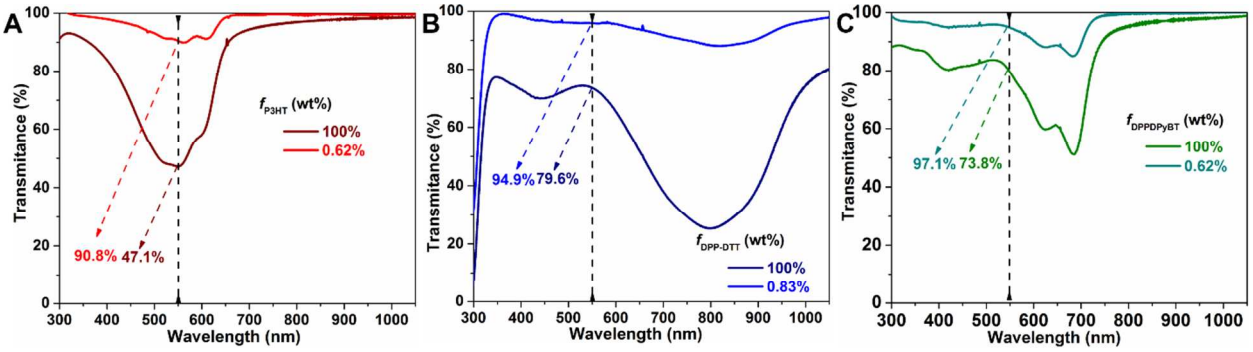

Fig. S5. Transmittance of the neat semiconductor films (thickness: P3HT: 30 ± 5.1 nm, DPP-DTT: 45 ± 3.7 nm, DPPDPyBT: 50 ± 4.2 nm.) and the robust semiconducting films under optimized condition (thickness: P3HT (0.49%): 1500 ± 30 nm, DPP-DTT (0.83%): 1350 ± 25 nm, DPPDPyBT (0.62%): 1425 ± 23 nm.)

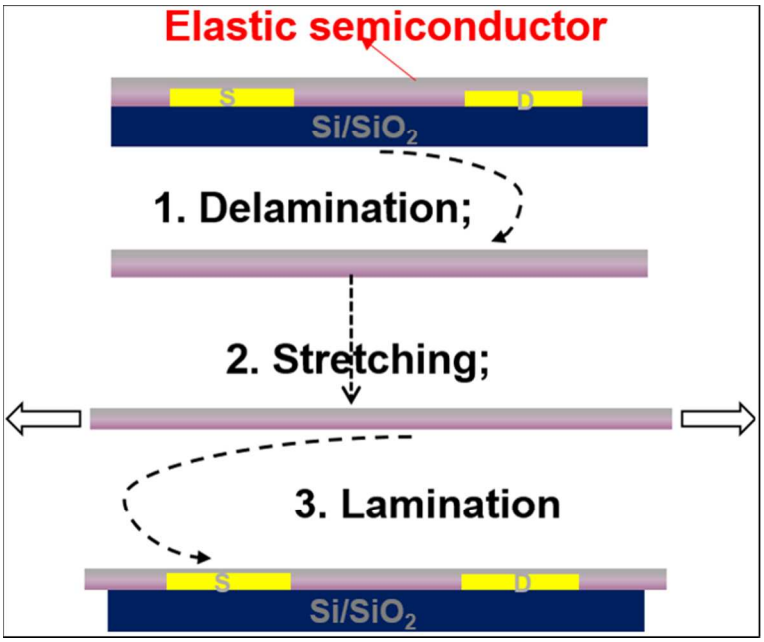

Fig. S6. A delamination-stretching-relamination process whereby semiconducting films were fabricated on OFET substrates, and then delaminated, stretched and finally while stretched, relaminated back onto an OFET substrate, was used to evaluate the electrical performance of the elastic semiconducting films under strain.

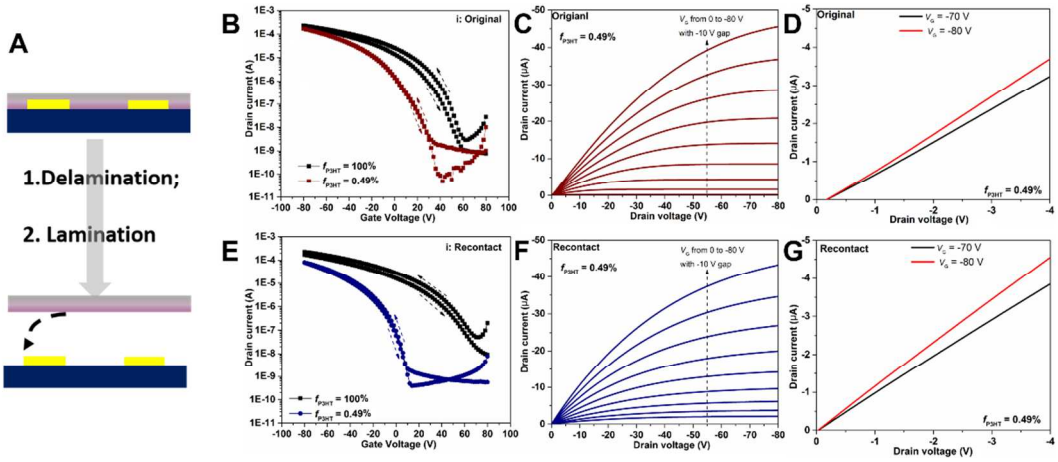

Fig. S7. Good contact between the semiconducting film and bottom contact electrodes during the delamination-lamination process is observed according to the reference method 11. Schematic illustration of the process of a semiconducting film delamination-lamination to the BGBC transistor (**A**). Transfer and output curves of the model films (f_{P3HT} = 0.49%) before delamination (**B** and **C**) and after lamination (E and F) on BGBC transistor devices. Output curves with low drain (-4 V) were collected through a detail scan and show linear characteristics for the ohmic contact (**D** and **G**).

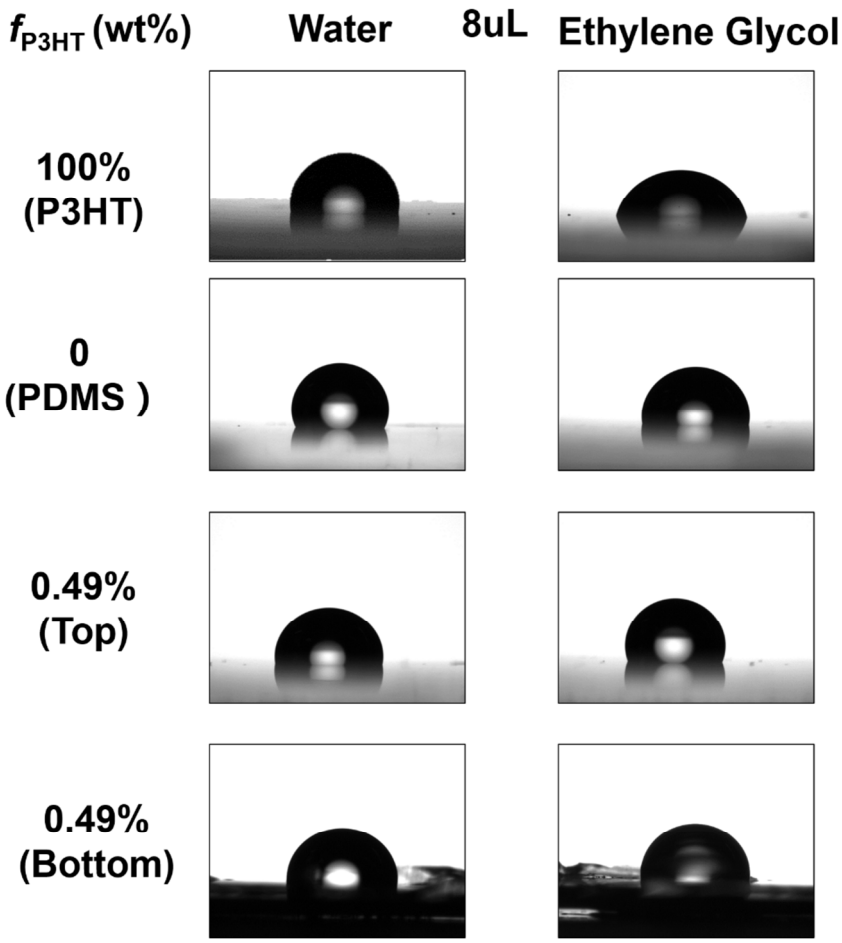

Fig. S8. Optical images showing the contact angles of the neat P3HT, neat PDMS, and top and bottom interface of P3HT/PDMS with 0.49 P3HT films.

Table S1. Surface free energy of neat P3HT, neat PDMS and top and bottom interface of P3HT/PDMS with 0.49% P3HT films in this paper. Calculated according to the Owens-Wendt method 12.

f_{P3HT} (wt%)	Contact angle (°)		Surface free energy (mJ/m^2)		
	H_2O	Ethylene Glycol	γ_S	γ_S^d	γ_S^p
100 (P3HT)	101.0 ± 0.5	76.3 ± 0.2	20.9 ± 0.5	19.3 ± 0.7	1.6 ± 0.2
0 (PDMS)	116.9 ± 0.4	101.4 ± 0.3	8.4 ± 0.2	7.3 ± 0.3	1.1 ± 0.1
0.49 (Top)	114.9 ± 0.7	100.9 ± 1.2	8.3 ± 0.4	6.0 ± 1.1	2.3 ± 0.1
0.49 (Bottom)	113.4 ± 1.7	98.7 ± 1.3	13.7 ± 0.2	10.6 ± 0.5	3.1 ± 0.4

Table S2. Solubility of P3HT and PDMS in selected organic solvents. Good solvents defined as solvents which can dissolve more than 5 mg/mL of the polymer, were assigned a value of “1”, while poor solvents were assigned a value of “0”.

Solvents	P3HT (mg/mL)	PDMS (mg/mL)
Chloroform	> 5	> 5
o-Dichlorobenzene	>5	<1
Trichloroethylene	>5	> 5
1,2,4-Trichlorobenzene	>5	<1
Chlorobenzene	>5	> 5
Carbon Disulfide	>5	<1
Heptane	<1	> 5
Tetrahydrofuran (THF)	<4	> 5
Toluene	<5	> 5
p-Xylene	<3	> 5
Hexane	<1	> 5
Dimethyl Sulfoxide (DMSO)	<1	<1
Dimethyl Formamide (DMF)	<1	<1
N-Methyl-2-Pyrrolidone (NMP)	<1	<1
Acetonitrile	<1	<1
Acetone	<1	<1
Cyclohexanone	<1	> 5
Methanol	<1	<1
Pyridine	<1	<1
Water	<1	<1

Table S3. Solubility parameters of selected organic solvents 13, 14.

Solvents	δ_D ($MPa^{1/2}$)	δ_P ($MPa^{1/2}$)	δ_H ($MPa^{1/2}$)
Chloroform	17.8	3.1	5.7
o-Dichlorobenzene	19.2	6.3	3.3
Trichloroethylene	18	3.1	5.3
1,2,4-Trichlorobenzene	20.2	4.2	3.2
Chlorobenzene	19	4.3	2
Carbon Disulfide	19.9	5.8	0.6
Tetrahydrofuran (THF)	16.8	5.7	8
Toluene	18	1.4	2
p-Xylene	17.8	1	3.1
Hexane	14.9	0	0
Dimethyl Sulfoxide (DMSO)	18.4	16.4	10.2
Dimethyl Formamide (DMF)	17.4	13.7	11.3
N-Methyl-2-Pyrrolidone (NMP)	18	12.3	7.2
Acetonitrile	15.3	18	6.1
Acetone	15.5	10.4	7
Cyclohexanone	17.8	8.4	5.1
Methanol	14.7	12.3	22.3
Pyridine	19	8.8	5.9

Table S4. Hansen solubility parameters of P3HT and PDMS and Flory-Huggins interaction parameters (χ) for P3HT/PDMS in $CHCl_3$. Abbott and Hansen software was used to determine HSPs following a previous reported method 15, 16. Interaction parameters (χ) were calculated from the solubility parameters according to a previous reported method 17.

	δ_D ($MPa^{1/2}$)	δ_P ($MPa^{1/2}$)	δ_H ($MPa^{1/2}$)	R_o ($MPa^{1/2}$)	R_a ($MPa^{1/2}$)	RED	x
P3HT	18.84	4.52	3.22	3.60	3.53	0.98	$x_{P3HT\text{-}CHCl3}$: 0.45
PDMS	16.37	4.10	2.69	5.80	4.27	0.74	$x_{PDMS\text{-}CHCl3}$:0.36
P3HT-PDMS	-	-	-	-	-	-	$x_{P3HT\text{-}PDMS}$: 0.55

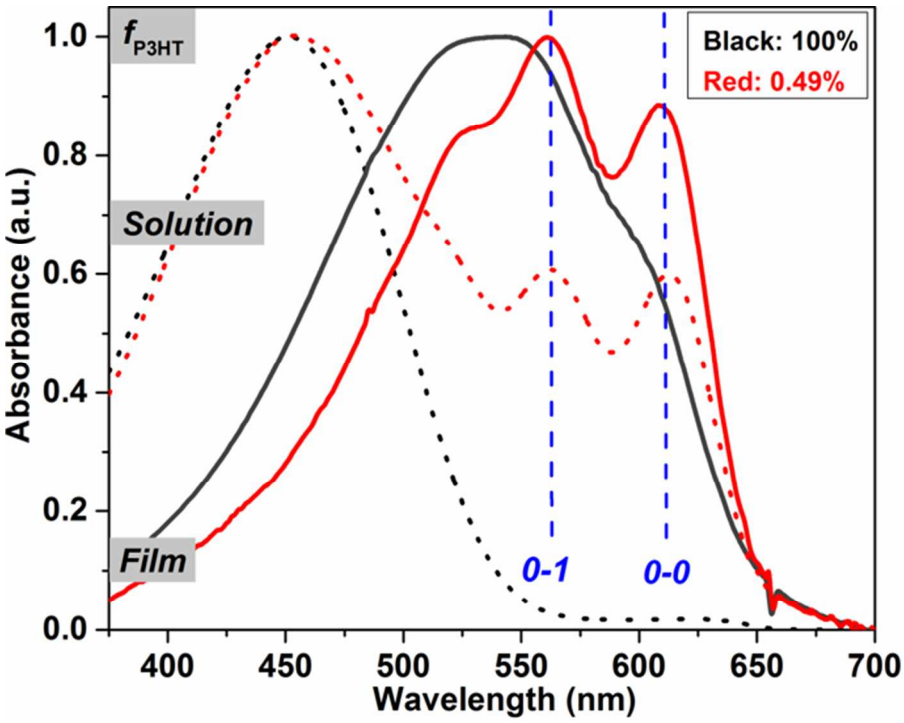

Fig. S9. Normalized UV-visible absorption of neat P3HT (black color) and P3HT/PDMS with 0.49% P3HT (red color): solution state (dot line) and film state (solid line). The free exciton bandwidth and percent of ordered aggregates were calculated according to Spano's model 18.

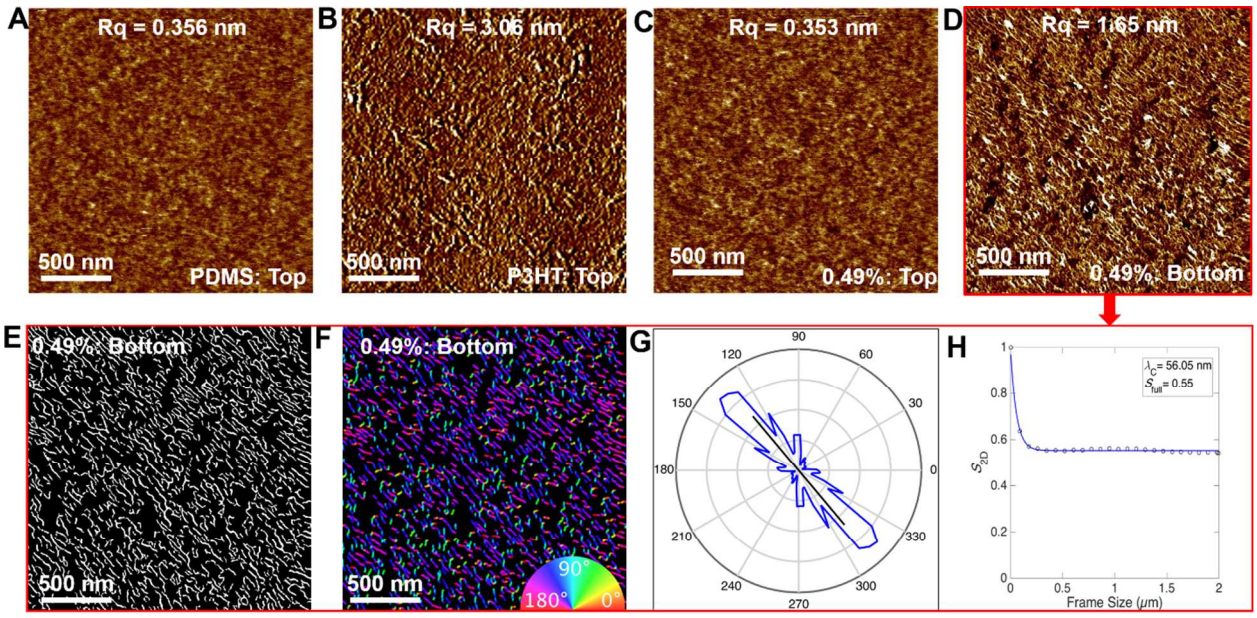

Fig. S10. AFM phase images of the neat P3HT (**A**), neat PDMS (**B**), and top (**C**) and bottom (**D**) interface of the P3HT/PDMS film with 0.49% P3HT. AFM image analysis (**E**: skeletonization and **F**: orientation map), polar plot (**G**), and orientational order parameter (S_{2D}, **H**) of the bottom interface P3HT/PDMS film with 0.49% P3HT based its AFM phase image. The RGB and binary images were collected through an open-source image-processing algorithm by analyzing their nanofiber orientation distribution and degree of nanofiber alignment 19. The S_{2D} was calculated according to a previous reported method 20, 21.

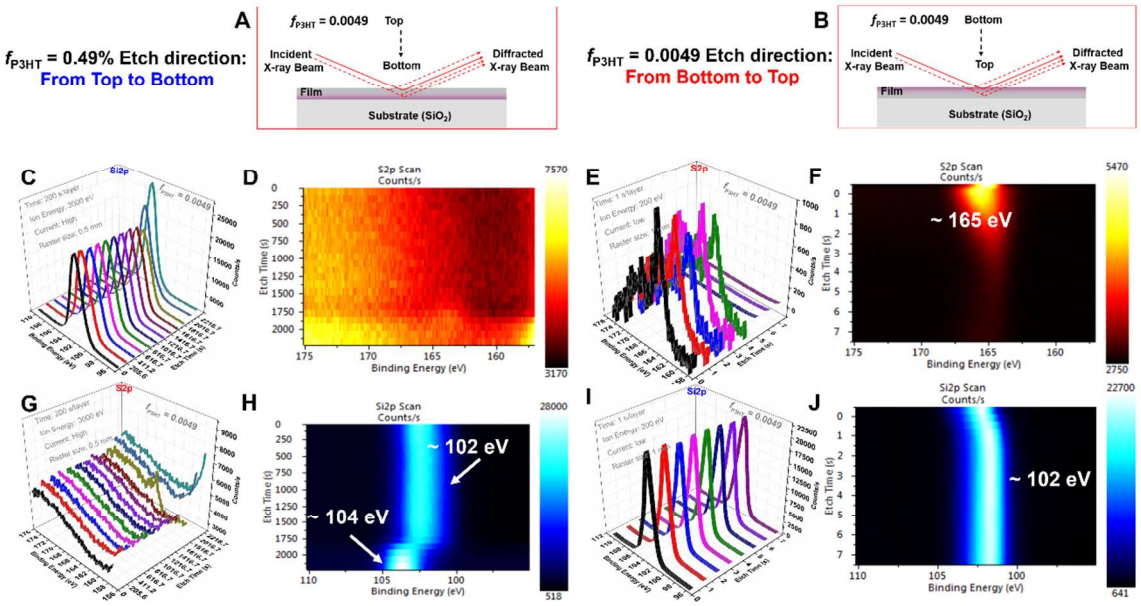

Fig. S11. Schematic illustration of the XPS of the P3HT/PDMS film with 0.49% P3HT etching direction: **A**: from top to bottom, **B**: from bottom to top). XPS spectra obtained at different depths in opposite etching direction, showing the changes of the Si 2p peak (**C** and **I**) and S 2p peak (**G** and **E**) at different depths. XPS color images obtained from the XPS spectra via a Fourier transformation, showing the S 2p (**D** and **F**) and Si 2p (**H** and **J**) elements distribution along the etching direction.

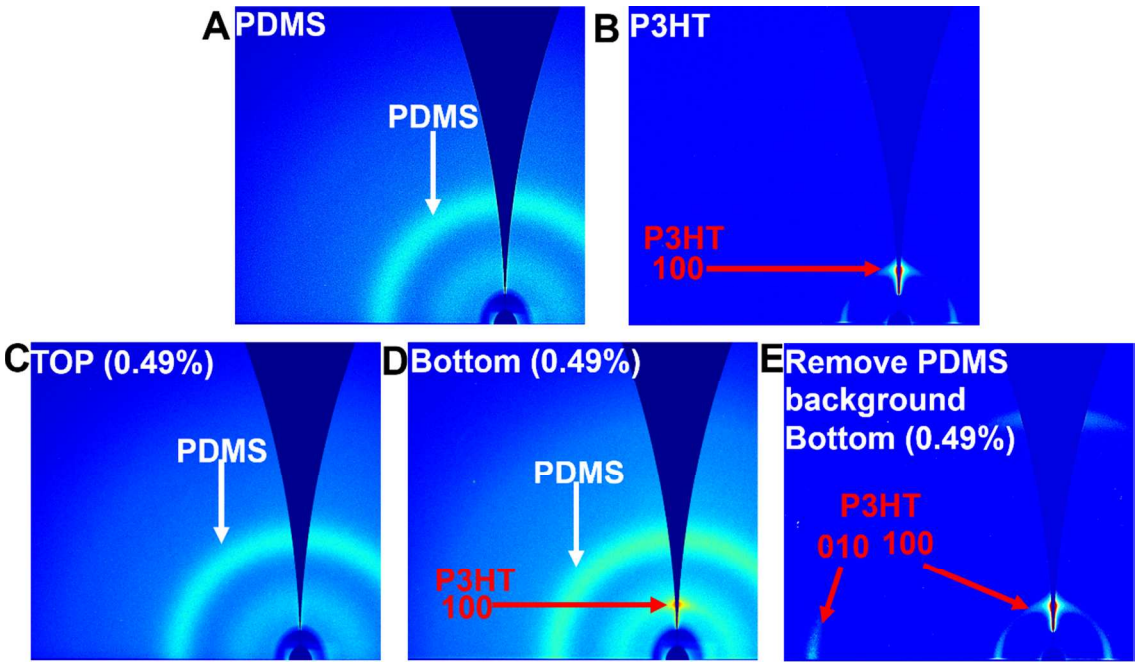

Fig. S12. Two-dimensional GIWAXS maps show the crystalline quality of the neat PDMS (**A**), neat P3HT (**B**), top (**C**) and bottom (**D**) interface of P3HT/PDMS film with 0.49% P3HT, and after removing the PDMS phase background (**E**) of P3HT/PDMS film with 0.49% P3HT.

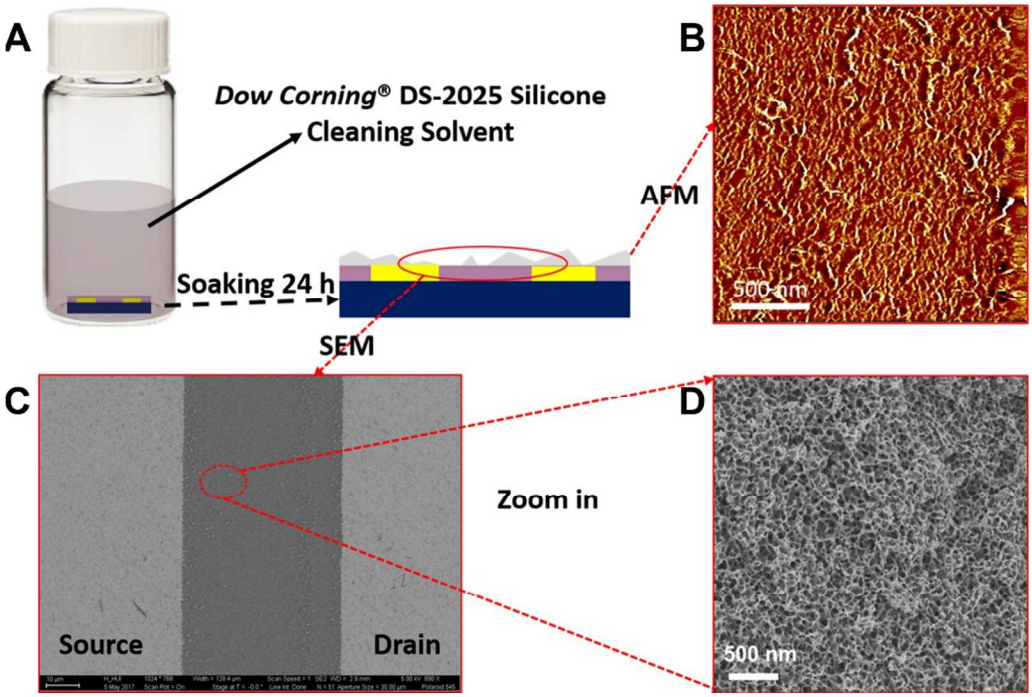

Fig. S13. Schematic illustration of the removing PDMS component via a commercial solvent (**A**). AFM (**B**) and SEM (**C**) images of P3HT/PDMS film with 0.49% P3HT after selectively removing PDMS with commercial solvents. The magnified SEM image clearly show the networked structure (**D**).

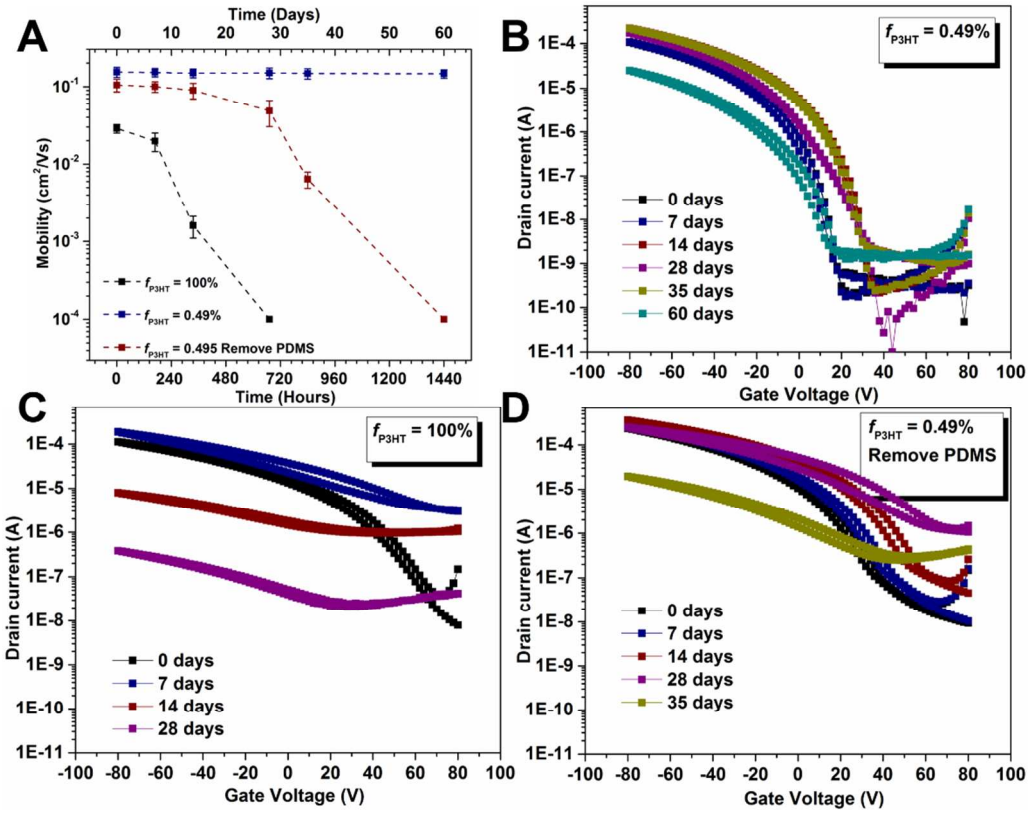

Fig. S14. Average charge carrier mobilities obtained from P3HT/PDMS film with 0.49% P3HT (blue navy color), neat P3HT (black color), P3HT/PDMS film with 0.49% P3HT after selectively removing PDMS (red wine color) as a function of air exposure time (**A**). Transfer characteristics of P3HT/PDMS film with 0.49% P3HT (**B**), neat P3HT **(C**), and P3HT/PDMS film with 0.49% P3HT after selectively removing PDMS (**D**) with different air exposure time.

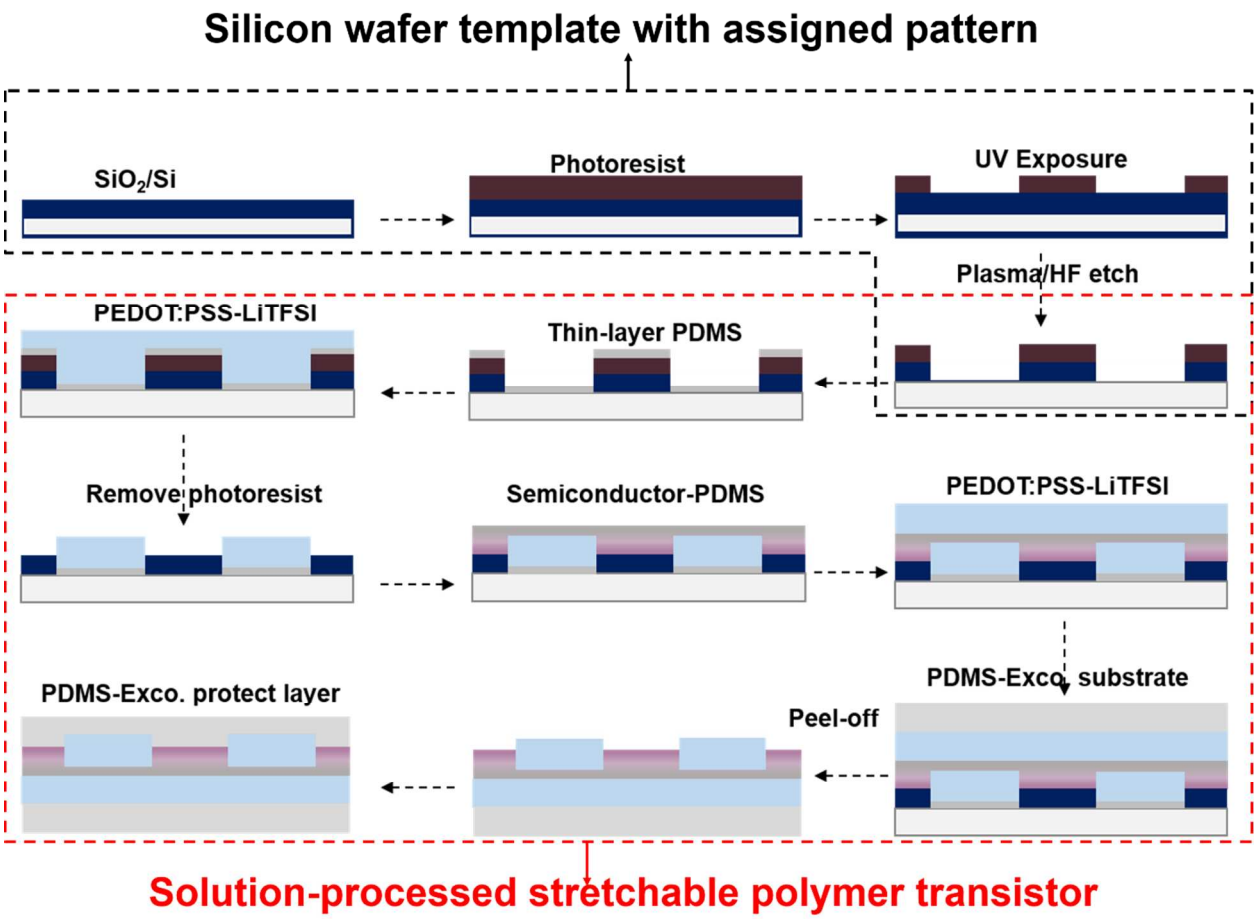

Fig. S15. Schematic illustration of the fabrication process for fully stretchable device via a solution processing based approach. The process begins with a 10 × 10 cm^2 silicon wafer with designed pattern and sacrificial layer. To ensure the one-step peel-off process could be realized, a thin-layer (10-20 nm) PDMS film was spin-coated and acted as an intermediate adhering layer between the substrate and electrodes due to their weakly-adhensive interface. The PEDOT:PSS-LiTFSI solution was spin-coated on the top of the PDMS adhesion layer and then dipped in acetone that dissolves the photoresist layer to leave a patterned PEDOT:PSS-LiTFSI and bare silicon dioxide surface. Semiconductor/PDMS solution and PEDOT:PSS-LiTFSI solution were sequencely spin-coated onto that layer to form a self-encapsulating active-dielectric layer and gaye electrode layer. The PDMS-Eco. solution was poured onto the top of the device, followed by 4 h curing at 55 ^{o}C. Finally, the source-drain electrode layer, active-dielectric layer together with the gate electrode layer were peeled off with the substrate from the wafer.

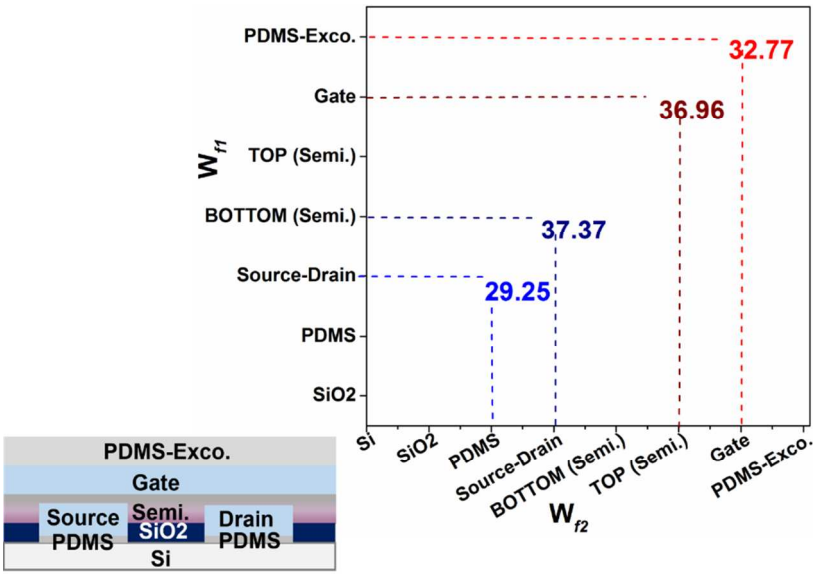

Fig. S16. Works of adhesion between the various layer involved in the fabrication process.

Table S5. Works of adhesion at the various interfaces involved in the fabrication process.

$W_{f1/f2}$ (mJ/m^2)	Si	SiO_2	PDMS	PEDOT:PSS-LiTFSI (Source-Drain)	PDMS-Semi. (Bottom)	PDMS-Semi. (Top)	PEDOT:PSS-LiTFSI (Gate)	PDMS-Eco.
Si	-	-	-	35.9	-	-	-	-
SiO2	-	-	-	44.2	-	-	-	-
PDMS	-	-	-	29.2	-	-	-	-
PEDOT:PSS-LiTFSI (Source-Drain)	35.9	44.2	29.2	-	37.37	-	-	-
PDMS-Semi. (Bottom)	-	-	-	37.37	-	-	-	-
PDMS-Semi. (Top)	-	-	-	-	-	-	39.96	-
PEDOT:PSS-LiTFSI (Gate)	-	-	-	-	-	39.96	-	32.77

PDMS-Eco.	-	-	-	-	-	-	32.77	-

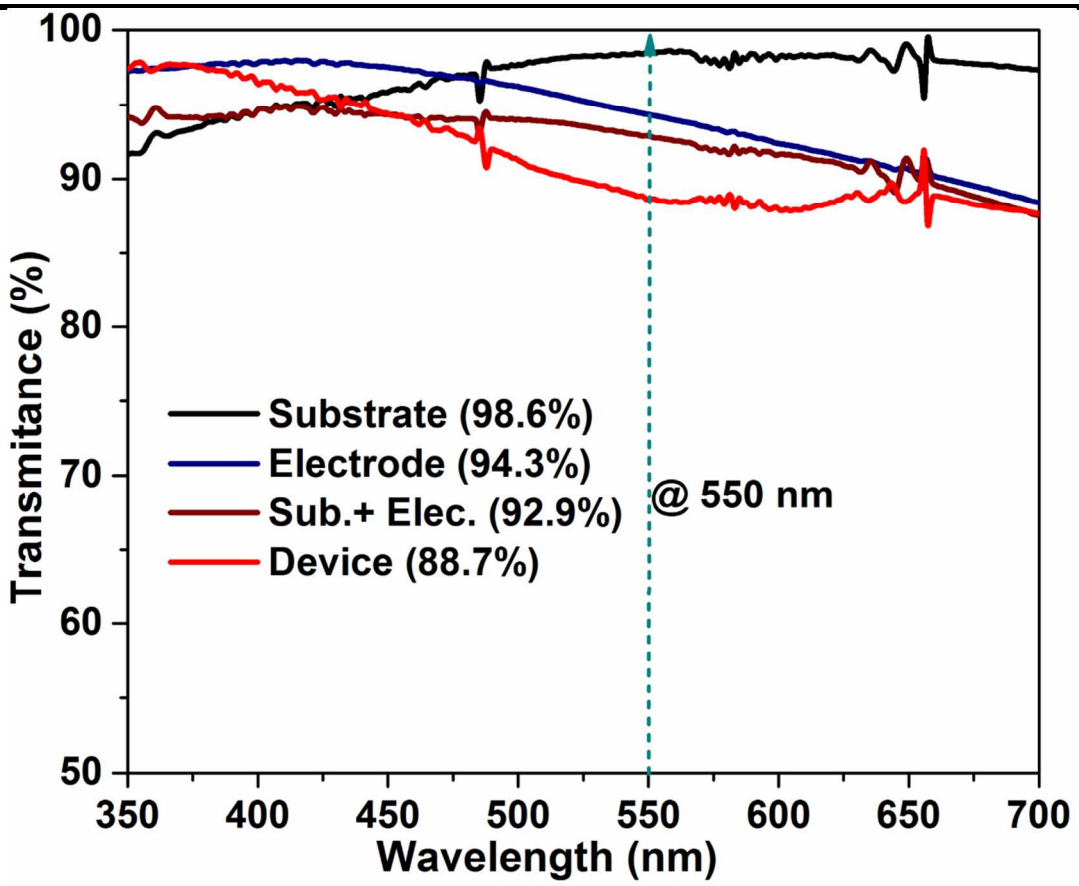

Fig. S17. Transmittance of the substrate (black line), electrode (blue navy line), and electrode on substrate (red wine line), and a transistor with all the components (semiconducting film: P3HT/PDMS film with 0.49% P3HT, red line).

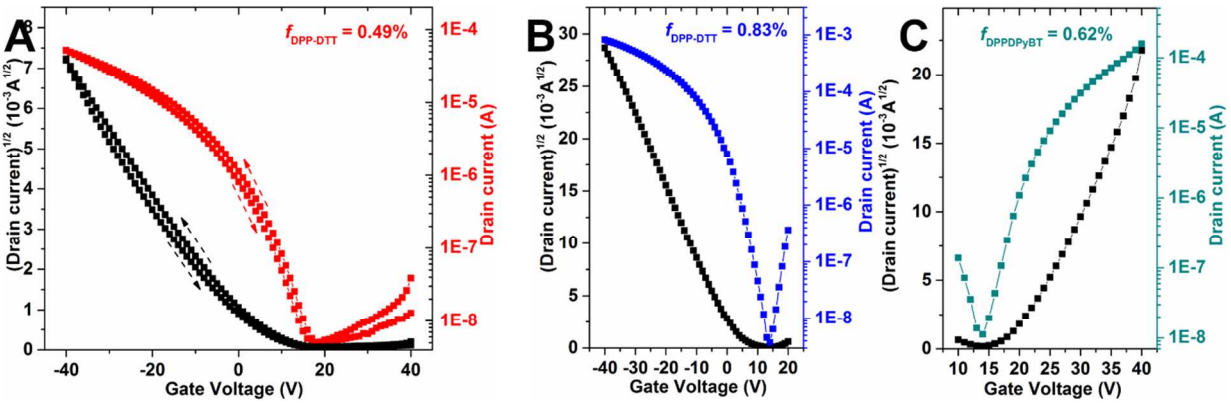

Fig. S18. Transfer curves obtained from the semiconducting films in their original condition: P3HT-PDMS (0.49%, A), DPP-DTT/PDMS (0.83 %, B) and DPPDPyBT/PDMS (0.62%, C).

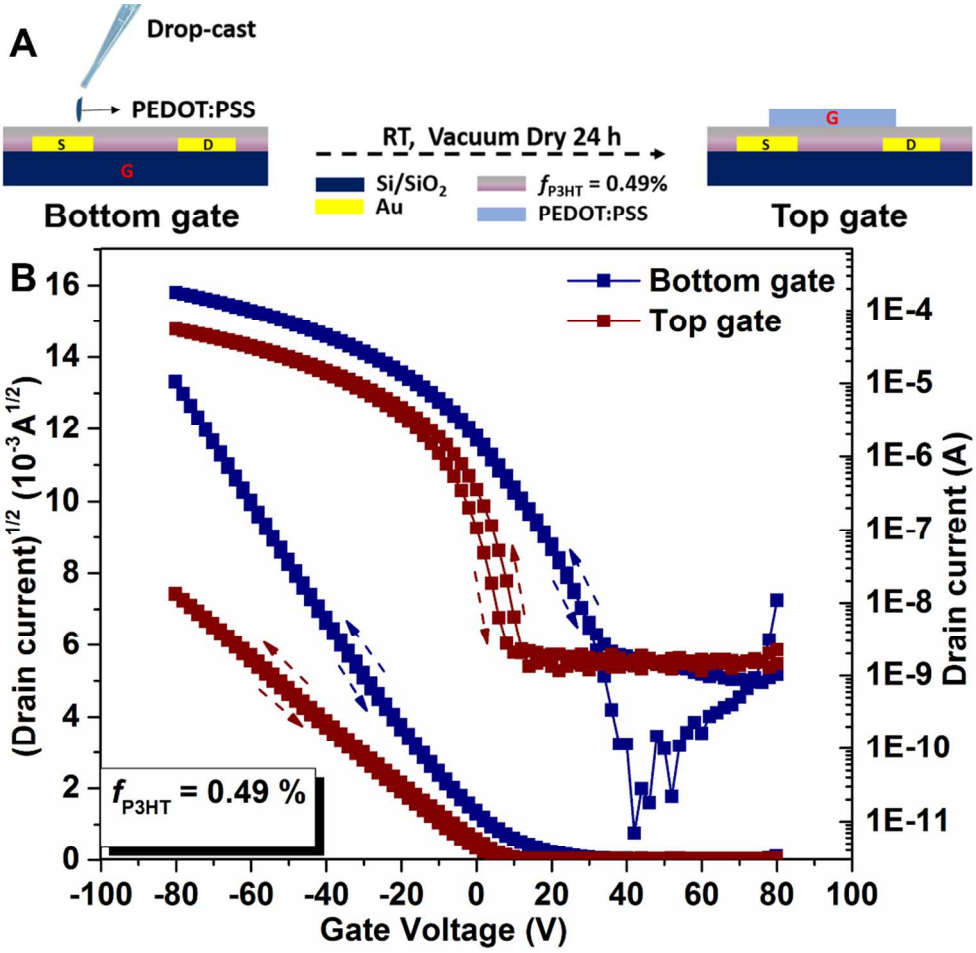

Fig. S19. Schematic illustration of the fabrication process for the top gate bottom contact transistors based on a bottom gate bottom contact transistors (**A**). Transfer curves of the transistors with two different device configuration: top gate (red wine color) and bottom gate (blue navy color) with the same semiconducting layer different dielectric layers (**B**).

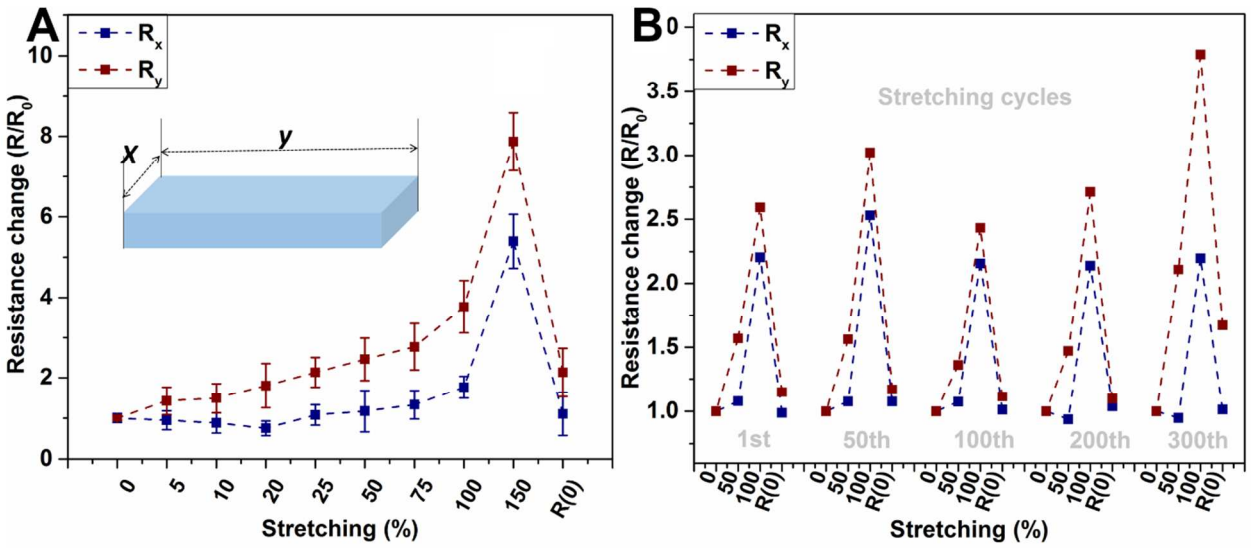

Fig. S20. Resistance change of electrode films with strains up to 150%, both x and y direction (**A**). Changes in the resistance after multiple stretching-releasing cycles under strains (**B**).

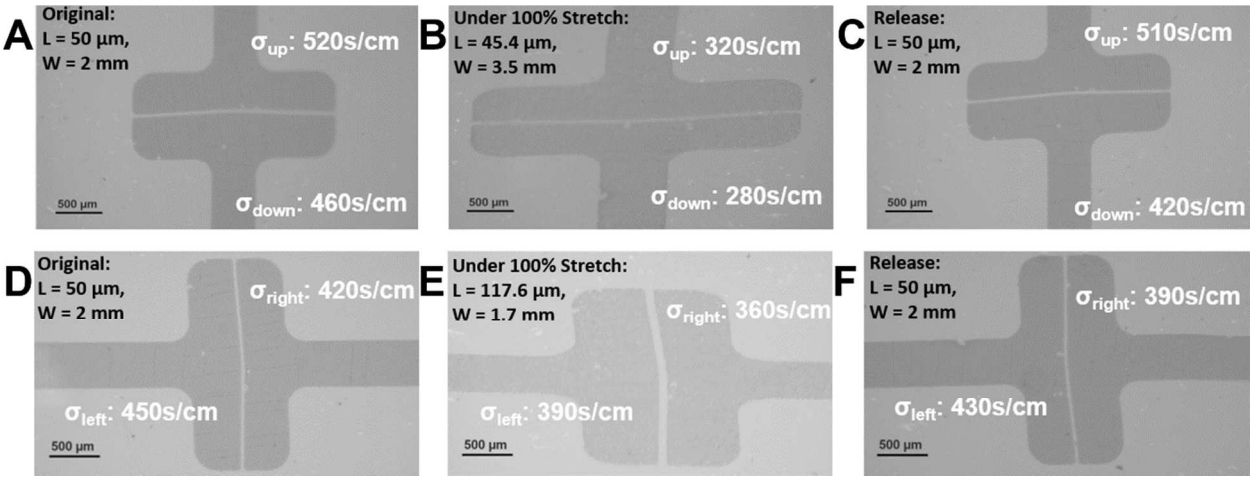

Fig. S21. Optical images show the changes in channel length and electrode conductivity in their original condition, 100% strain condition and release condition.

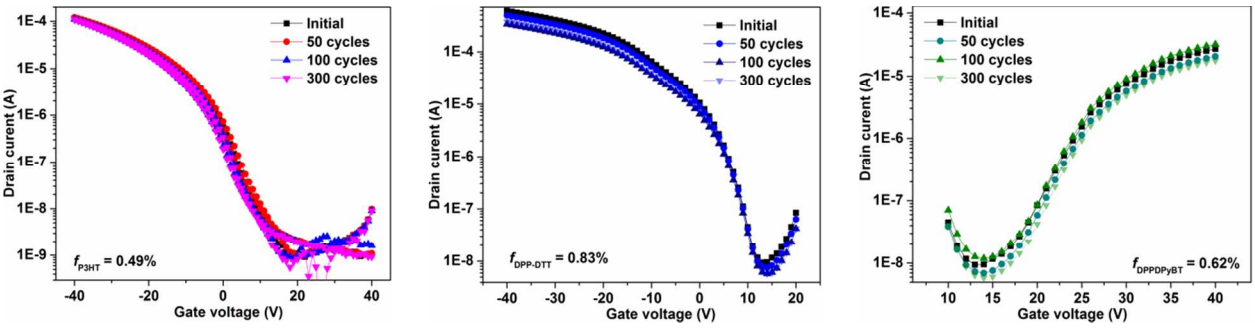

Fig. S22. Transfer curves from the fully stretchable transistor after multiple stretching-releasing cycles at 100% strain along the charge transport direction.

Table S6. Measured device geometry, channel size, electrode conductivity, dielectric capacitance and mobility in the fully stretchable transistor in their original condition, 100% strain condition and release condition.

Stretching direction	Channel Length (μm)	Channel Width (μm)	Conductivity (S/cm)		Capacitance (nF/cm^2)	Mobility (cm^2/Vs)
			Left/Up	Right/Down		
Original	50	2000	~ 500	~ 450	1.58	0.1253
Parallel channel 100% strain	117.6	1700	~390	~ 360	2.01	0.0921
Perpendicular channel 100% strain	45.4	3500	~320	~ 280	2.01	0.0753
Release	50	2000	~500	~400	1.58	0.1156

Video:

Video S1. Freestanding semiconducting film (0.49 wt% of P3HT) under sequential stretching, twisting and poking.

Video S2. Video showing the stretchable high visual transparency of the transistor arrays.

Video S3. Fully stretchable transistor array fabrication process.

Video S3: Fully stretchable transistor array fabrication process

1. The device fabrication started with a Si/SiO_2 wafer with the desired electrode pattern which was prepared in cleanroom.
   Detail: Silicon wafers coated with 30 nm of silicon dioxide (SiO_2) were purchased from Rogue Valley Microdevices. Microposit primer composed of hexamethyldisilane (HMDS) was spin coated onto the substrate followed by Microposit S1813 photoresist at 3000 RPM for 30 seconds. The coated substrate was soft baked at 115°C for 4 minutes. Using conventional photolithographic techniques, the wafer with a photomask was exposed to 405 nm UV light for approximately 9 seconds and subsequently developed in MF-319 Developer for 1 and a half minutes (c). This produced a pattern for the electrodes that were 2 cm long and separated by 50 microns. The wafer was placed in 6:1 BOE with a measured SiO2 etch rate of 770 angstrom/minute, for 5 minutes (d).
2. PDMS solution (20 mg/mL in $CHCl_3$) was spin coated (2000 rpm, 30 s) onto the wafer as an adhesion layer and cured in a vacuum oven at 100 ^oC for 30 min.
3. PEDOT: PSS-LiTFSI solution was prepared as reported previously and spin-coated (1000 rpm, 60 s) onto the wafer. The film was dried at 120 ^oC for 10 min.
4. The photoresist layer was removed using acetone, leaving only the PEDOT: PSS-LiTFSI on the PDMS adhesion layer.
5. Semiconductor/PDMS mixtures were subsequently spin-coated (1500 rpm, 60 s) onto these layers to form a self-encapsulating active material-dielectric layer.
6. Gate electrodes were prepared by spin-coating (1500 rpm, 60 s) PEDOT: PSS-LiTFSI solution onto the above layers.
7. Then a mixture with 15 wt% of PDMS in Ecoflex gel (w_{partA}:w_{partB} = 1:1) was poured onto the top the device.
8. The samples cured at 55 °C for 4 h.
9. Finally, the source-drain electrode layer, active material-dielectric layer together with the gate electrode layer were peeled off with the PDMS/Ecoflex substrate from the Si wafer.
10. Fully transparent stretchable transistor array was thereby achieved.

References

1. Wang Y, et al. (2017) A highly stretchable, transparent, and conductive polymer. Science Advances 3(3).

2. Shin M, et al. (2015) Polythiophene Nanofibril Bundles Surface-Embedded in Elastomer: A Route to a Highly Stretchable Active Channel Layer. Advanced Materials 27(7):1255-1261.

3. Song E, et al. (2016) Stretchable and Transparent Organic Semiconducting Thin Film with Conjugated Polymer Nanowires Embedded in an Elastomeric Matrix. Advanced Electronic Materials 2(1):1500250-n/a.

4. Goffri S, et al. (2006) Multicomponent semiconducting polymer systems with low crystallization-induced percolation threshold. Nat Mater 5(12):950-956.

5. Lu G, et al. (2013) Moderate doping leads to high performance of semiconductor/insulator polymer blend transistors. Nature Communications 4:1588.

6. Qiu L, et al. (2008) Versatile Use of Vertical-Phase-Separation-Induced Bilayer Structures in Organic Thin-Film Transistors. Advanced Materials 20(6):1141-1145.

7. Kumar A, Baklar MA, Scott K, Kreouzis T, Stingelin-Stutzmann N (2009) Efficient, Stable Bulk Charge Transport in Crystalline/Crystalline Semiconductor–Insulator Blends. Advanced Materials 21(44):4447-4451.

8. Root SE, Savagatrup S, Printz AD, Rodriquez D, Lipomi DJ (2017) Mechanical Properties of Organic Semiconductors for Stretchable, Highly Flexible, and Mechanically Robust Electronics. Chemical Reviews.

9. Rodriquez D, et al. (2017) Comparison of Methods for Determining the Mechanical Properties of Semiconducting Polymer Films for Stretchable Electronics. ACS Applied Materials & Interfaces 9(10):8855-8862.

10. Owens DK & Wendt RC (1969) Estimation of the surface free energy of polymers. Journal of Applied Polymer Science 13(8):1741-1747.

11. Anonymous Solvent Compatibility of Poly(dimethylsiloxane)-Based Microfluidic Devices.

12. Machui F, Abbott S, Waller D, Koppe M, & Brabec CJ (2011) Determination of Solubility Parameters for Organic Semiconductor Formulations. Macromolecular Chemistry and Physics 212(19):2159-2165.

13. Duong DT, et al. (2012) Molecular solubility and hansen solubility parameters for the analysis of phase separation in bulk heterojunctions. Journal of Polymer Science Part B: Polymer Physics 50(20):1405-1413.

14. Anonymous (17-<66286_fm.pdf>.

15. Shepherd WEB, et al. (2010) Aggregate formation and its effect on (opto)electronic properties of guest-host organic semiconductors. Applied Physics Letters 97(16):163303.

16. Murphy JN, Harris KD, & Buriak JM (2015) Automated Defect and Correlation Length Analysis of Block Copolymer Thin Film Nanopatterns. PLOS ONE 10(7):e0133088.

17. Jordens S, Isa L, Usov I, & Mezzenga R (2013) Non-equilibrium nature of two-dimensional isotropic and nematic coexistence in amyloid fibrils at liquid interfaces. Nature Communications 4:1917.

18. Persson NE, McBride MA, Grover MA, & Reichmanis E (2017) Automated Analysis of Orientational Order in Images of Fibrillar Materials. Chemistry of Materials 29(1):3-14.

19. Choi D, et al. (2016) Elastomer–Polymer Semiconductor Blends for High-Performance Stretchable Charge Transport Networks. Chemistry of Materials 28(4):1196-1204.

20. Chen NC, et al. (2004) Modified transmission line model and its application to aluminum ohmic contacts with n-type GaN. Applied Physics Letters 84(14):2584-2586.

21. Chang M, Choi D, Fu B, & Reichmanis E (2013) Solvent Based Hydrogen Bonding: Impact on Poly(3-hexylthiophene) Nanoscale Morphology and Charge Transport Characteristics. ACS Nano 7(6):5402-5413.